Electronic Supplementary Material (ESI) for Sustainable Energy & Fuels.
This journal is © The Royal Society of Chemistry 2024

Efficient electrochemical water oxidation catalyzed by N_4-coordinated nickel complexes under neutral condition

Zhijun Ruan,[a] Jinfeng Dong,[a] Jieying Wang,[a] Zhichao Qi,[a] Xiaoli Chen,[*a] Xiangming Liang,[*b] Junqi Lin[*a]

[a] Hubei Key Laboratory of Processing and Application of Catalytic Materials, College of Chemistry and Chemical Engineering, Huanggang Normal University, Huanggang 438000, China. E-mail: 872802461@qq.com; linjunqi@hgnu.edu.cn

[b] School of Basic Medical Sciences, Ningxia Medical University, Yinchuan 750004, China. E-mail: liangxm@nxmu.edu.cn

Table S1 Crystal data and structure refinement for **1**.

Identification code	$[Ni(dmabpy)](ClO_4)_2$	
Empirical formula	$C_{16}H_{21}Cl_2N_4NiO_8$	
Formula weight	526.98	
Temperature	280(2) K	
Wavelength	0.71073 Å	
Crystal system	Orthorhombic	
Space group	$P2_12_12_1$	
Unit cell dimensions	a = 11.789(4) Å	$\alpha = 90°$
	b = 13.176(5) Å	$\beta = 90°$
	c = 13.461(7) Å	$\gamma = 90°$
Volume	2090.9(15) $Å^3$	
Z	4	
Density (calculated)	1.674 Mg/m^3	
Absorption coefficient	1.236 mm^{-1}	
F(000)	1084	
Crystal size	0.23 × 0.35 × 0.27 mm	
Theta range for data collection	2.163 to 24.982°.	
Index ranges	-14<=h<=14	
	-14<=k<=14	
	-15<=l<=15	
Reflections collected	45583	
Independent reflections	3392 [R(int) = 0.1637]	
Completeness to theta = 24.982°	92.6 %	
Absorption correction	Semi-empirical from equivalents	
Max. and min. transmission	0.7452 and 0.6193	
Refinement method	Full-matrix least-squares on F^2	
Data / restraints / parameters	3392/0/284	
Goodness-of-fit on F^2	1.043	
Final R indices [I>2sigma(I)]	$R^1 = 0.0542$, $wR^2 = 0.1324$	
R indices (all data)	$R^1 = 0.0892$, $wR^2 = 0.1618$	
Absolute structure parameter	0.58(5)	
Extinction coefficient	n/a	
Largest diff. peak and hole	0.521 and -0.472 e.$Å^{-3}$	

$R_1 = \Sigma||F_o| - |F_c||/\Sigma|F_o|$, $wR_2 = [\Sigma(|Fo|^2 - |Fc|^2)^2/\Sigma(Fo_2)]^{1/2}$

Table S2 Crystal data and structure refinement for **2**.

Identification code	$[Ni(mabpy)](ClO_4)_2$
Empirical formula	$C_{14}H_{18}Cl_2N_4NiO_8$
Formula weight	499.93
Temperature	306(2) K
Wavelength	0.71073 Å
Crystal system	Monoclinic
Space group	$P2_1/c$
Unit cell dimensions	a = 13.430(6) Å α = 90° b = 9.197(3) Å β = 110.543° c = 16.247(7) Å γ = 90°
Volume	1879.1(13) $Å^3$
Z	4
Density (calculated)	1.767 Mg/m^3
Absorption coefficient	1.370 mm^{-1}
F(000)	1024
Crystal size	0.27 × 0.29 × 0.33 mm
Theta range for data collection	2.588 to 25.079°.
Index ranges	-16<=h<=16 -10<=k<=10 -19<=l<=19
Reflections collected	39204
Independent reflections	3310 [R(int) = 0.0936]
Completeness to theta = 25.079°	99.5 %
Absorption correction	Semi-empirical from equivalents
Max. and min. transmission	0.7452 and 0.6755
Refinement method	Full-matrix least-squares on F^2
Data / restraints / parameters	3310/0/263
Goodness-of-fit on F^2	1.060
Final R indices [I>2sigma(I)]	R_1 = 0.0420, wR_2 = 0.0984
R indices (all data)	R_1 = 0.0603, wR_2 = 0.1069
Extinction coefficient	n/a
Largest diff. peak and hole	0.546 and -0.593 e.$Å^{-3}$

$R_1 = \Sigma||F_o| - |F_c||/\Sigma|F_o|$, $wR_2 = [\Sigma(|Fo|^2 - |Fc|^2)^2/\Sigma(Fo_2)]^{1/2}$

Table S3 Selected bond lengths (Å) and angles (deg) for complex **1**–**2**.

Complex	**1**	**2**
Bond length (Å)		
Ni1–N1	1.837(16)	1.819(3)
Ni1–N2	1.836(14)	1.820(3)
Ni1–N3	2.075(15)	1.913(4)
Ni1–N4	2.035(16)	1.940(3)
Bond angles (deg)		
N1–Ni1–N2	94.6(3)	83.41(14)
N2–Ni1–N3	71.4(6)	84.67(17)
N3–Ni1–N4	120.4(3)	107.27(16)
N4–Ni1–N1	73.0(7)	84.97(13)

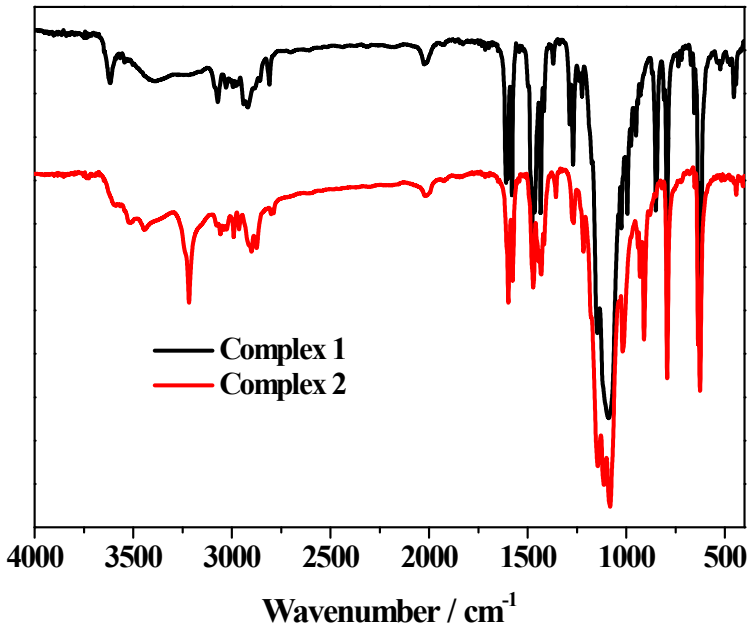

Fig. S1 Infrared spectrum of complex [Ni(dmabpy)]$(ClO_4)_2$ (**1**) and [Ni(mabpy)]$(ClO_4)_2$ (**2**).

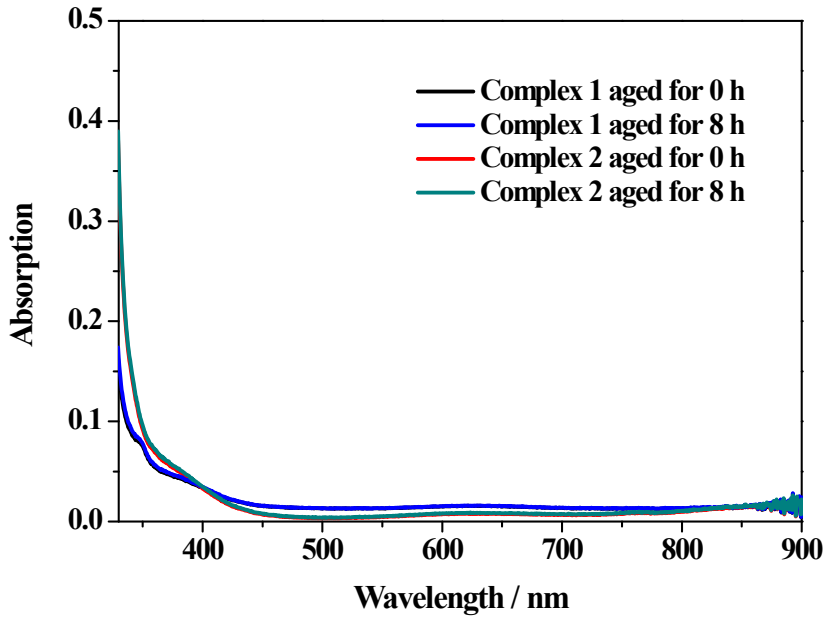

Fig. S2 Time-dependent UV-vis absorption spectra of 1 mM complex **1** (b) and **2** (d) in 0.1 M phosphate buffer solution (PBS) at pH 7.0.

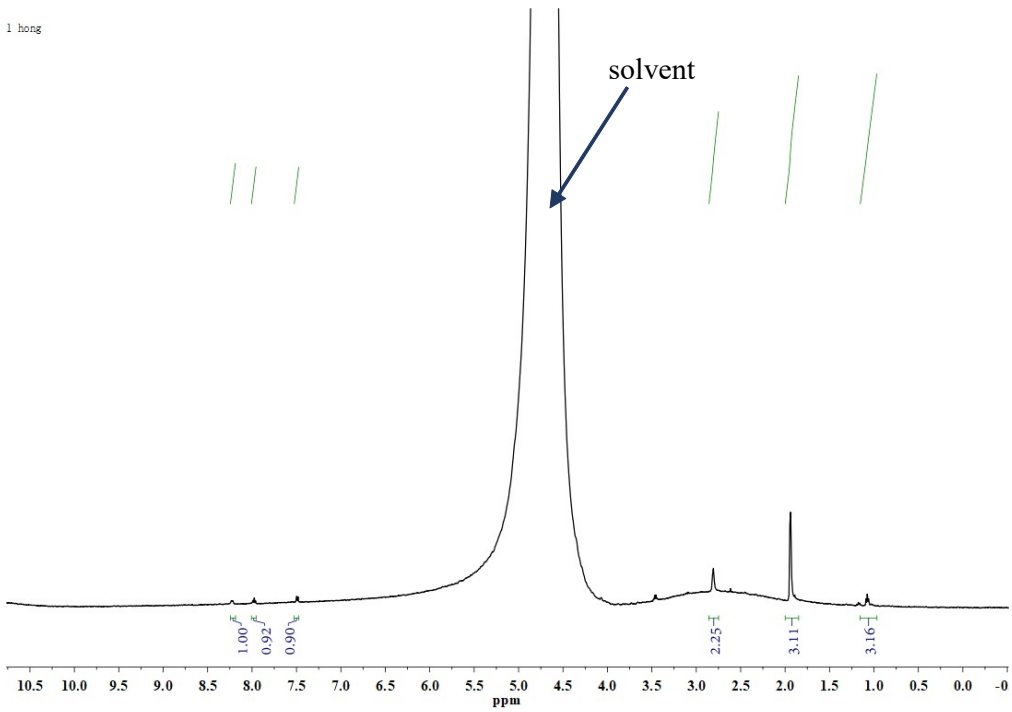

Fig. S3 The ^{1}H NMR spectrum of Complex **1** (400 MHz, D_2O). δ 8.24 (d, 2H, CH_{py}), 7.98 (t, 2H, CH_{py}), 7.51 (m, 2H, CH_{py}), 2.76 (s, 4H, CH_2), 1.93 (s, 6H, CH_3), 1.08 (s, 6H, CH_3).

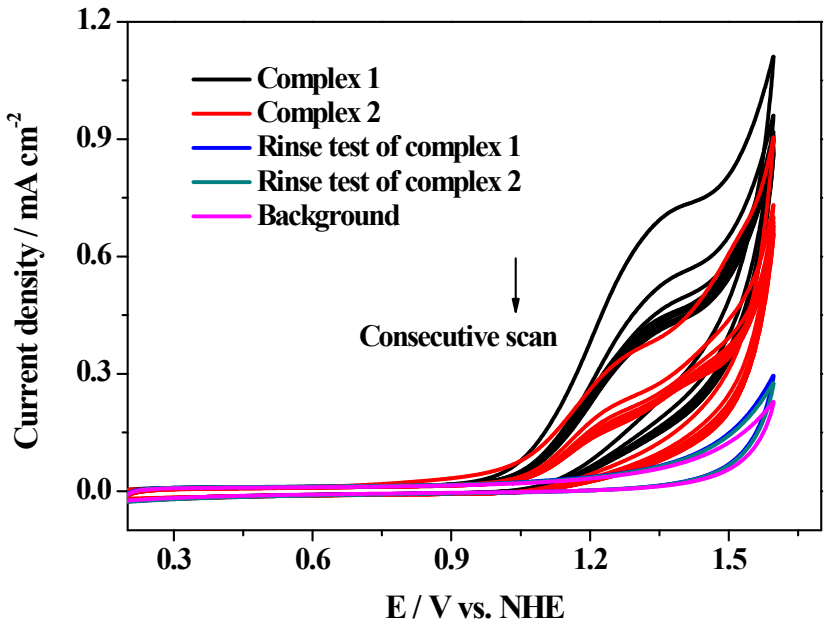

Fig. S4 Consecutive cyclic voltammograms of 1 mM complex **1** and **2** at 100 mV/s using GC electrode at 0.1 M pH 7.0 PBS. The CV from a rinse test after 20 scans and the background CV in the absence of complex is shown.

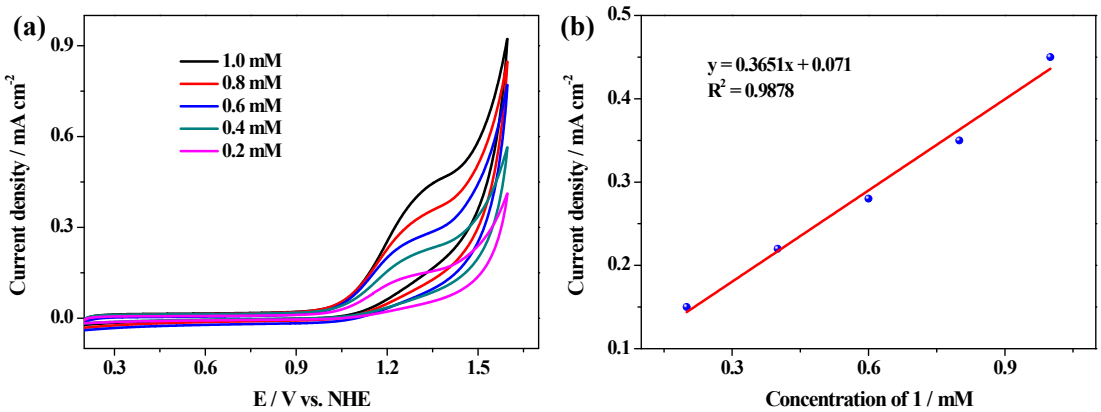

Fig. S5 Cyclic voltammograms of various concentration of **1** in 0.1 M PBSs at pH 7.0 with scan rate of 100 mV s^{-1} (a) and the dependence of catalytic current density of catalytic wave on the concentration of **1** in 0.1 M PBSs at pH 7.0 (b).

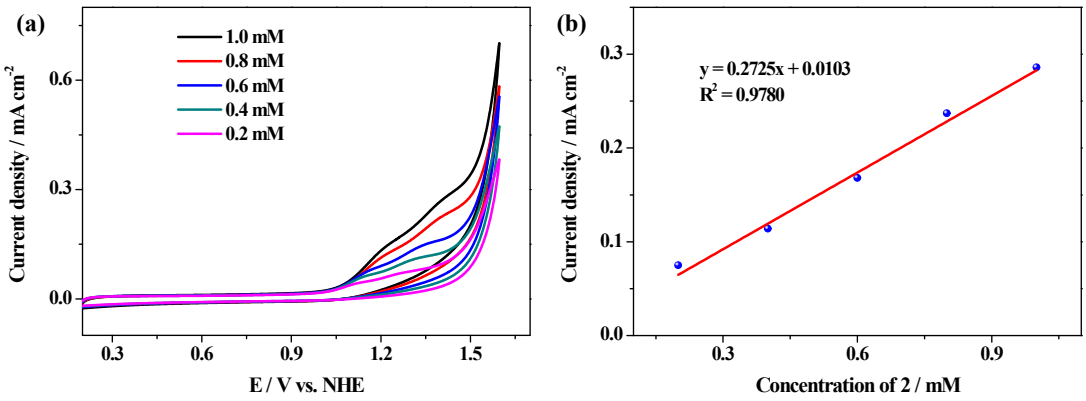

Fig. S6 Cyclic voltammograms of various concentration of **2** in 0.1 M PBSs at pH 7.0 with scan rate of 100 mV s^{-1} (a) and the dependence of catalytic current density of catalytic wave on the concentration of **2** in 0.1 M PBSs at pH 7.0 (b).

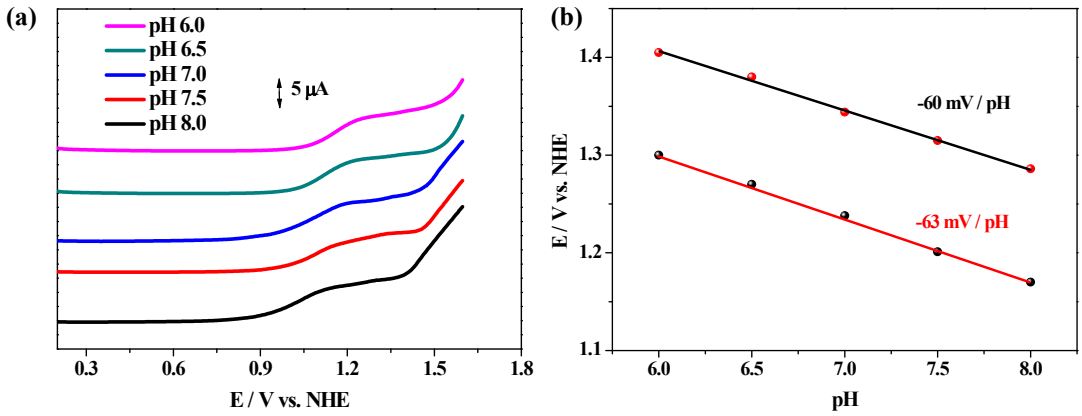

Fig. S7 DPV test of 1 mM complex **1** in 0.1 M PBS at various pH values (a) and the relationship between the potential of each redox couple of complex **1** and the pH value of electrolyte (b).

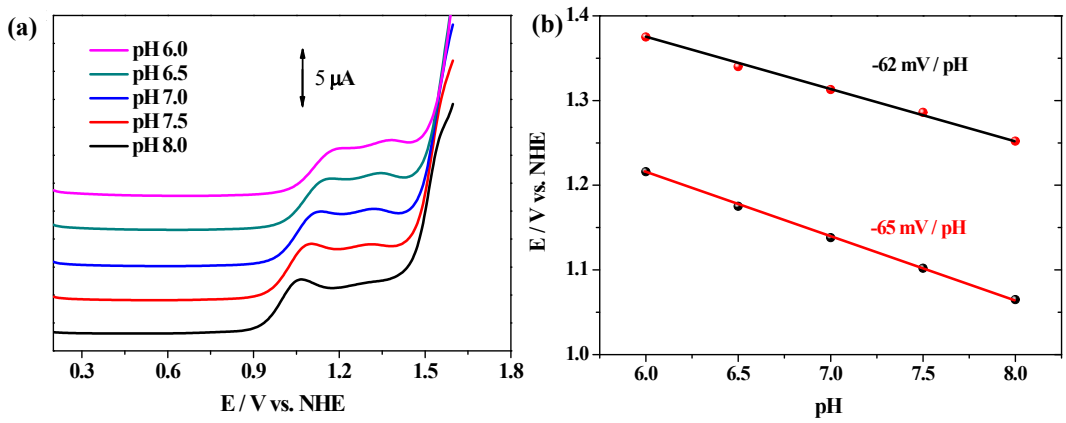

Fig. S8 DPV test of 1 mM complex **2** in 0.1 M PBS at various pH values (a) and the relationship between the potential of each redox couple of complex **2** and the pH value of electrolyte (b).

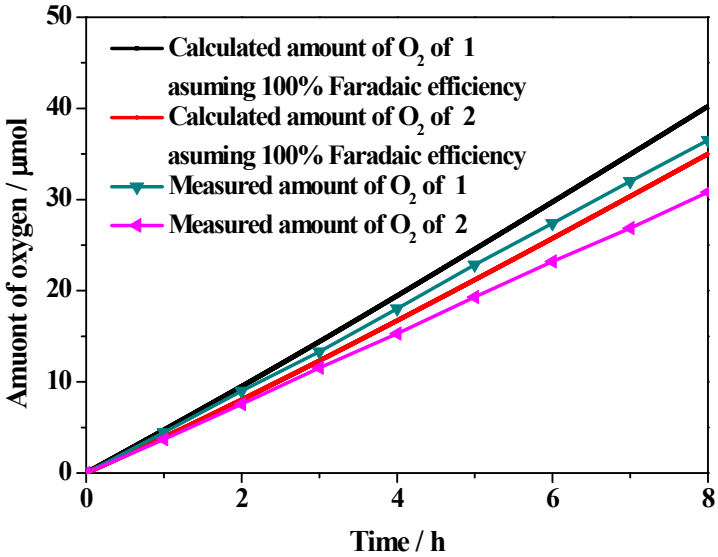

Fig. S9 Faradaic efficiency of O_2 evolution for complex **1** and **2** under 8 h of electrolysis at 1.50 V vs. NHE in 0.1 M PBS at pH 7.0.

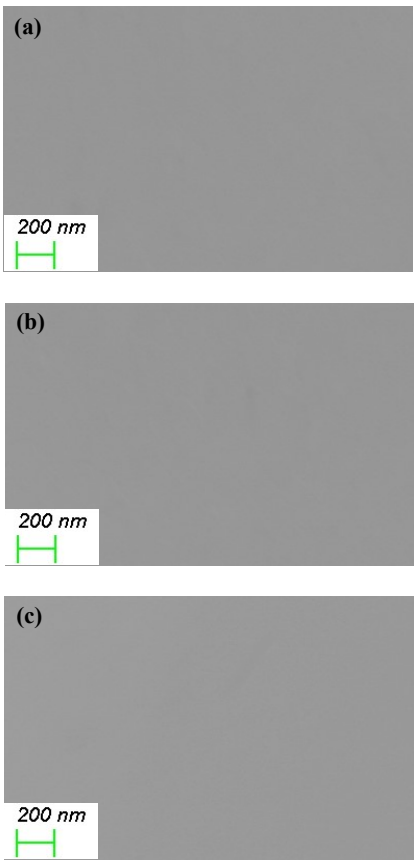

Fig. S10 SEM images of the surface of ITO electrode before (top) and after 8 h CPE experiments (1.50 V vs. NHE) of 1 mM of **1** (b) and **2** (c) in 0.1 M neutral PBS.

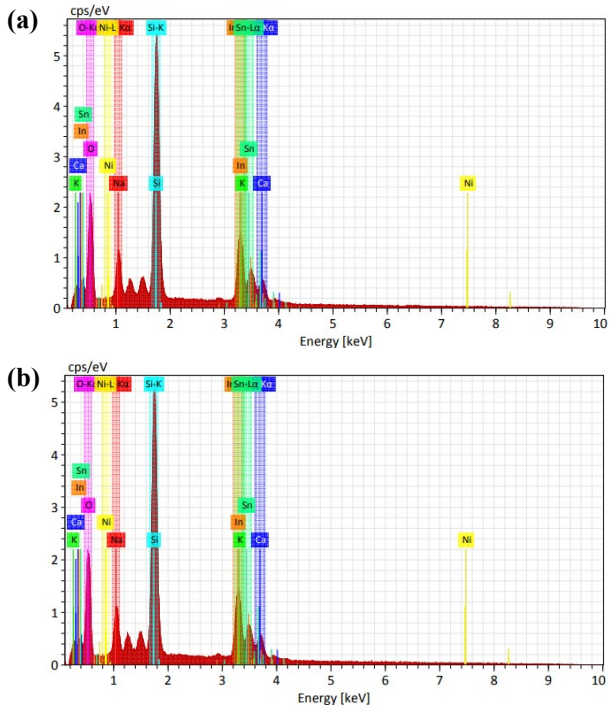

Fig. S11 EDX analysis of the surface of ITO electrode after 8 h CPE experiments of 1 mM of **1** (a) and **2** (b) in 0.1 M neutral PBS.

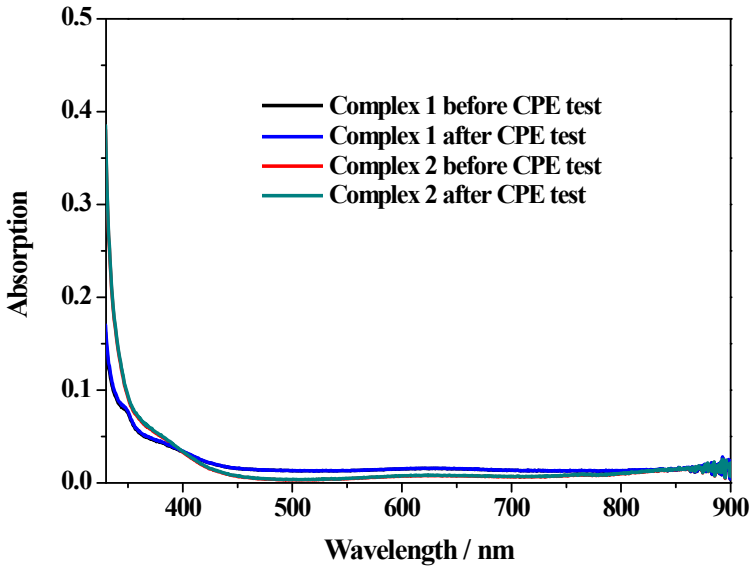

Fig. S12 UV-vis absorption spectra of 1 mM of complex **1** and **2** before and after controlled potential electrolysis in neutral buffer solution.

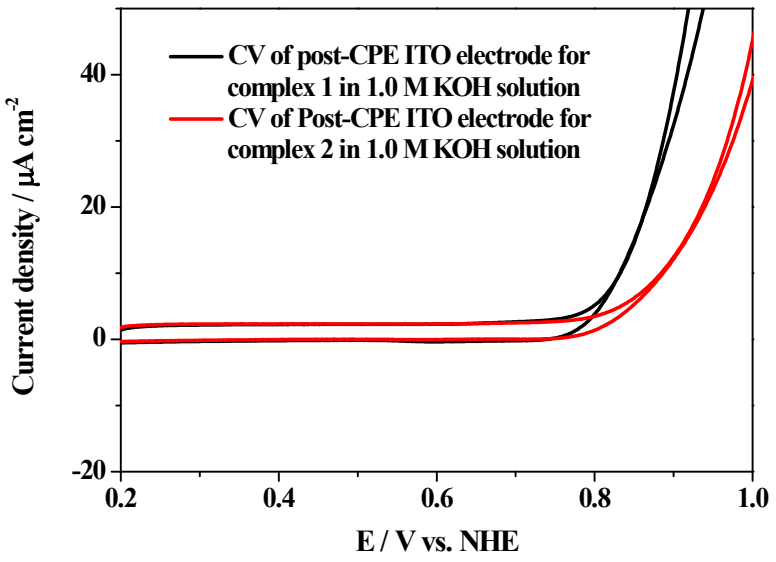

Fig. S13 CV test of post-CPE test ITO electrode for complex **1** and **2** in 1.0 M KOH solution.

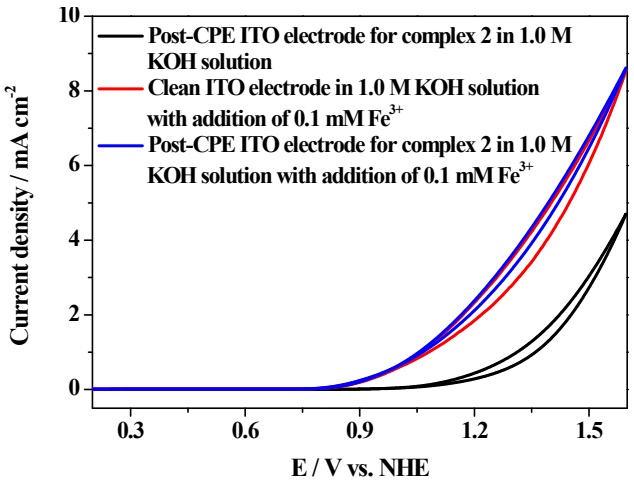

Fig. S14 CV test of post-CPE test ITO electrode for complex **2** in 1.0 M KOH solution, clean ITO electrode in 1.0 M KOH solution with addition of 0.1 mM Fe^{3+} and post-CPE test ITO electrode for complex **2** in 1.0 M KOH solution with addition of 0.1 mM Fe^{3+}.

Table S4 Onset overpotential of **1**, **2** and some reported Ni based mononuclear molecular WOC

Catalyst	pH	η/mV [a]	Ref.
$[Ni(meso\text{-}L^1)]^{2+}$	7.0	170	S1
$[Ni(TMC)(CH_3CN)]^{2+}$	7.0	483	S2
$[Ni(mcp)(H_2O)_2]^{2+}$	7.0	480	S3
$[Ni(L)(H_2O)_2]^{2+}$	6.5	533	S4
$[Ni^{II}\text{-}L1]^{2+}$	7.0	580	S5
Ni-Porphyrin	7.0	380	S6
$[Ni(tpen)]^{2+}$	8.0	440	S7
Ni-PY5	10.8	800	S8
$[Ni(bptn)(H_2O)]^{2+}$	9.0	351	S9
$[Ni(mbptn)(CH_3CN)]^{2+}$	9.0	401	S9
$[Ni(tmbptn)(H_2O)]^{2+}$	9.0	581	S9
$[Ni(TAML)]^{2-}$	7.0	680	S10
$[NiL]^{2+}$	9.0	550	S11
$[Ni(dmabpy)](ClO_4)_2$	7.0	473	This work
$[Ni(mabpy)](ClO_4)_2$	7.0	573	This work

[a] η = Onset overpotential

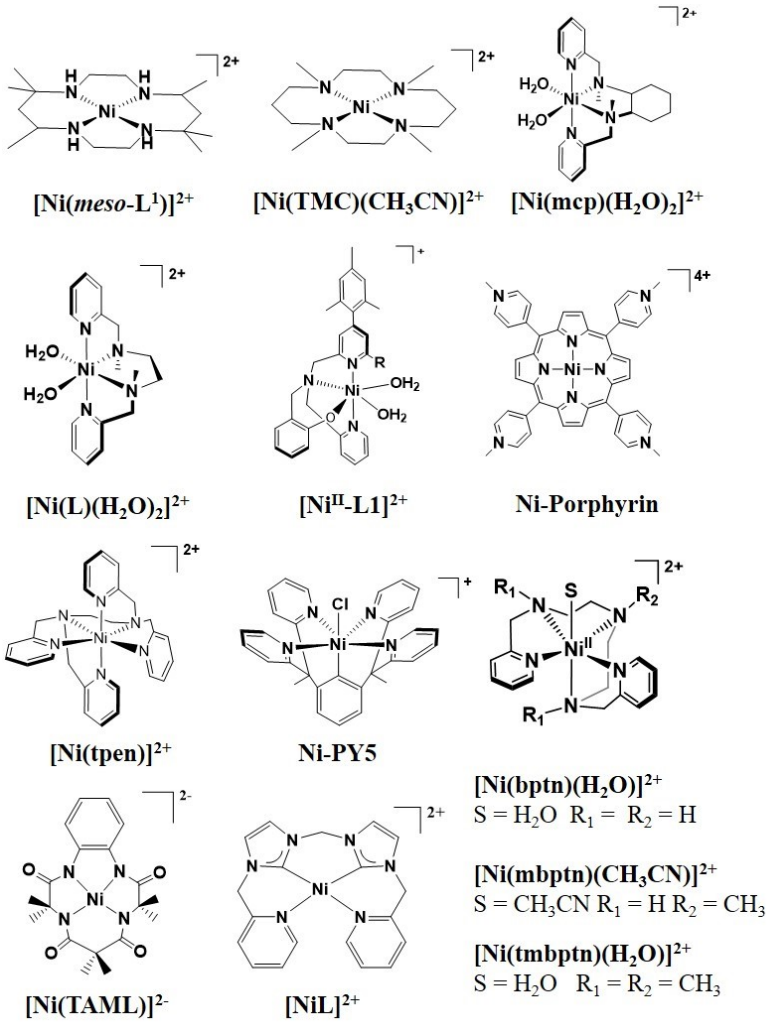

References

S1 M. Zhang, M.-T. Zhang, C. Hou, Z.-F. Ke and T.-B. Lu, *Angew. Chem., Int. Ed.*, 2014, 53, 13042–13048.

S2 L.-H. Zhang, F. Yu, Y. Shi, F. Li and H. Li, *Chem. Commun.*, 2019, **55**, 6122–6125.

S3 J.-W. Wang, X.-Q. Zhang, H.-H. Huang and T.-B. Lu, *ChemCatChem*, 2016, **8**, 3287–3293.

S4 G.-Y. Luo, H.-H. Huang, J.-W. Wang and T.-B. L, *ChemSusChem*, 2016, **9**, 485–491.

S5 D. Wang and C. O. Bruner, *Inorg. Chem.*, 2017, **56**, 13638–13641.

S6 Y. Han, Y. Wu, W. Lai and R. Cao, *Inorg. Chem.*, 2015, **54**, 5604–5613.

S7 Q.-J. Li, Y.-J. Ren, Q. Xie, M. Wu, H.-X. Feng, L.-M. Zheng, H.-X. Zhang, J.-Q. Long and T.-S. Wang, *Appl. Organomet. Chem.*, 2020, **34**, e5813.

S8 L. Wang, L. Duan, R. B. Ambre, Q. Daniel, H. Chen, J. Sun, B. Das, A. Thapper, J.

Uhlig, P. Dinér and L. Sun, *J. Catal.*, 2016, **335**, 72–78.

S9 X. Chen, X. Liao, C. Dai, L. Zhu, L. Hong, X. Yang, Z. Ruan, X. Liang and J. Lin, *Dalton Trans.*, 2022, **51**, 18678–18684.

S10 H. Lee, X. Wu and L. Sun, *ChemSusChem*, 2020, **13**, 3277–3282.

S11 H. M. Shahadat, H. A. Younus, N. Ahmad, M. A. Rahaman, Z. A. K. Khattak, S. Zhuiykov and F. Verpoort, *Catal. Sci. Technol.*, 2019, **9**, 5651–5659.